materials

MDPI

Article

Self-Powered Photodetector Based on FTO/*n*-TiO_2/*p*-$CuMnO_2$ Transparent Thin Films

Carmen Lazau [1,†], Mircea Nicolaescu [1,2,†], Corina Orha [1,†], Viorel Şerban [2,3] and Cornelia Bandas [1,*]

[1] National Institute for Research and Development in Electrochemistry and Condensed Matter Timisoara, 300569 Timisoara, Romania; carmen.lazau@gmail.com (C.L.); nicolaescu.mircea13@yahoo.com (M.N.); orha.corina@gmail.com (C.O.)
[2] Department of Materials and Manufacturing Engineering, Faculty of Mechanical Engineering, University Politehnica of Timisoara, 300222 Timisoara, Romania; viorel.serban@upt.ro
[3] Romanian Academy of Technical Sciences, 300223 Timisoara, Romania
* Correspondence: cornelia.bandas@gmail.com
† These authors contributed equally to this work.

Abstract: A self-powered photodetector with the FTO/*n*-TiO_2/*p*-$CuMnO_2$ configuration, representing the novelty of the work, was successfully achieved for the first time and presumes two steps: deposition of the *n*-type semiconductor (TiO_2) by the doctor blade method and of the *p*-type semiconductor ($CuMnO_2$) by the spin coating technique, respectively. Investigation techniques of the structural and morphological characteristics of the as-synthesized heterostructures, such as XRD, UV-VIS analysis, and SEM/EDX and AFM morphologies, were used. The *I-t* measurements of the photodetector showed that the responsivity in the self-powered mode was 2.84×10^7 A W^{-1} cm^2 and in the 1 V bias mode it was 1.82×10^6 A W^{-1} cm^2. Additionally, a self-powered current of 14.2 nA was generated under UV illumination with an intensity of 0.1 mW/cm^2. Furthermore, under illumination conditions, the response time (t_{res}) and the recovery time (t_{rec}) of the sensor exhibited a good response; thus, t_{res} = 7.30 s and t_{rec} = 0.4 s for the self-powered mode, and in the 1 V bias mode, these were t_{res} = 15.16 s and t_{rec} = 2.18 s. The above results show that the transparent heterojunction device of *n*-TiO_2/*p*-$CuMnO_2$ exhibited a self-powered ultraviolet photodetector with high sensitivity.

Keywords: self-powered photodetector; *n*-TiO_2/*p*-$CuMnO_2$ heterojunction; thin film

Citation: Lazau, C.; Nicolaescu, M.; Orha, C.; Şerban, V.; Bandas, C. Self-Powered Photodetector Based on FTO/*n*-TiO_2/*p*-$CuMnO_2$ Transparent Thin Films. *Materials* **2022**, *15*, 5229. https://doi.org/10.3390/ma15155229

Academic Editors: Adrien Carretero-Genevrier and César Magén

Received: 5 July 2022
Accepted: 26 July 2022
Published: 28 July 2022

1. Introduction

Self-powered ultraviolet photodetectors (SPVs) have been widely studied lately because they have a great advantage; namely, they do not need any external power sources, can operate continuously and independently and do not require high costs to produce them [1]. The operating principle of photodetectors (PD) is very well known, being based on the conversion of photon energy into an electrical signal by photogenerated carriers [2–4]. The PD performance is mainly dependent on the properties of the semiconductor materials used, regarding their abilities to transform optical signals into electrical signals that are determined by a process of electron-hole pair generation and recombination within semiconductor materials [5]. Self-powered operation happens because of the photovoltaic effect, i.e., the photocurrent generated without applied bias, and requires a heterojunction to be formed in the device. In most cases, the dark current has high values, and thus power losses appear, this being a major disadvantage, leading to unwanted power losses [6]. In this way, to remove the mentioned inconveniences, UV photodetectors have been studied and developed that have the ability to detect UV radiation and produce an electric field, so they can be self-powered.

Over time, it was shown that metal oxide heterojunctions can facilitate photovoltaics for self-powered operation due to their built-in potential, low cost, non-toxicity and easy

synthesis methods [6]. Thus, a self-powered UV photodetector based on a *p*-*n* heterojunction has a main advantage due to its built-in potential that automatically separates generated electron-hole pairs [7]. Therefore, various metal oxide semiconductor materials (i.e., TiO_2, ZnO, CuO and NiO) have been applied for different types of photovoltaic cells [8,9], but from them, TiO_2 was selected as the most desirable material for photovoltaic devices [10]. B. Yin and coworkers developed an ultraviolet detector based on the FTO/TiO_2/MoO_3 heterojunction with potential well-trapping electrons under dark and demonstrated the excellent responsivity under UV illumination [11]. Furthermore, transparent photovoltaic cells and self-powered photodetectors were fabricated by a TiO_2/NiO heterojunction, with an excellent UV response in the photovoltaic mode and high transparency in the visible light region (about 57%) [12]. Z.M. Bai et al. reported a UV self-powered photodetector based on a ZnO nanowire array in which a high sensitivity of 475 without external bias was found [13]. Y. Xie and coworkers fabricated a self-powered UV detector based on single-crystalline rutile TiO_2 nanorod arrays grown directly on FTO and demonstrated a fast photoresponse speed, high photosensitivity, excellent spectral selectivity, low-cost fabrication and environmentally friendly characteristic [14]. Over time, copper-based delafossite-type metal oxides $CuMO_2$ (M = Mn, Fe, Cr, Al, Ga, In, B) have offered excellent properties that have attracted a great deal of attention, especially $CuMnO_2$, due to their excellent optical and electrical characteristics [15–17]. C.-L. Hsu et al. successfully obtained the configuration *p*-$CuMnO_2$/*n*-ZnO NW with excellent organic gas sensing and UV and visible light detection [18]. A study by Y. Zhang et al. demonstrated a self-powered UV photodetector based on heterojunction-type CuSCN/ZnO nanorods, with excellent stability and reproducibility characteristics [19]. R.R. Prabhu et al. reported the obtaining of a highly transparent and high conducting *p*-CuO/*n*-ZnO heterojunction, with applicability in the development of efficient and low-cost optoelectronic devices, particularly photodetectors, solar cells and gas sensors [20].

Based on our previous research in the field of the development of TiO_2-$CuMnO_2$ thin films obtained in different configurations and demonstrating the functionality of heterojunctions as well as the ability to detect UV radiation [21,22], the progress and novelty of this work is related to the design and fabrication of a self-powered and transparent UV photodetector with the FTO/*n*-TiO_2/*p*-$CuMnO_2$ heterojunction. A completely solution-processed transparent (>60%) *p*-*n* heterojunction has been fabricated in the structure FTO/*n*-TiO_2/*p*-$CuMnO_2$ and the performance of the photodetector under dark and UV illumination conditions is investigated. Finally, an increased performance during the self-powered mode (zero bias) as well as in the normal bias mode in terms of high responsivity, good recovery time and high sensitivity in 0 V bias was exhibited by the UV photodetector device.

2. Materials and Methods

2.1. Chemicals

All reagents were of analytical purity grade and used without further purification, as follows: titanium isopropoxide (TTIP, 98%), α-terpinol, ethyl cellulose, acetone, ethyl alcohol, fluorine-doped tin oxide (FTO, 99%), $Cu(NO_3)_2 \cdot 3H_2O$, $Mn(NO_3)_2 \cdot 4H_2O$, sodium hydroxide were purchased by Sigma-Aldrich Company (St. Louis, MO, USA).

2.2. Fabrication of FTO/n-TiO_2/p-$CuMnO_2$ Heterojunction Photodetector

The self-powered photodetector was achieved in several steps, as presented in the schematic diagram in Figure 1.

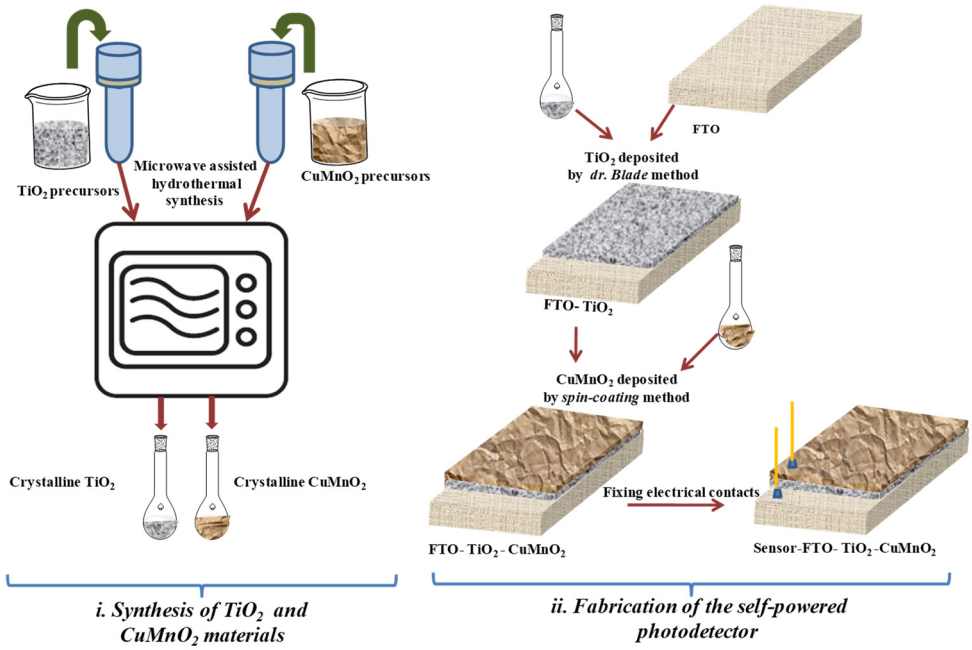

Figure 1. Schematic illustration of self-powered photodetector fabrication.

(i) Initially, TiO_2 and $CuMnO_2$ powders were synthesized by the microwave-assisted hydrothermal method. Therefore, for TiO_2 synthesis, the solution was obtained by mixing 40 mL of distilled water (DI) with 6 mL of TTIP under continuous stirring for 2 h. The solution was then introduced into a quartz autoclave with 50% degree of fullness and treated in a Multiwave 300 (*Anton Paar, 2.45 GHz*) microwave reaction system for 30 min at a temperature of 200 °C. On the other hand, the $CuMnO_2$ nanocrystalline compound was obtained as previously reported [23]. The $CuMnO_2$ powder used in this research was treated for 5 min at 180 °C in a microwave reaction system. After autoclaving, the synthesized samples (TiO_2 and $CuMnO_2$) were filtered, washed with distilled water and dried at 80 °C for 24 h. For thin film deposition, the TiO_2 and $CuMnO_2$ solutions were prepared, according to the following protocol: 0.2 g of TiO_2 powder and 0.1 g of $CuMnO_2$, respectively, were mixed with a matrix solution consisting of solution of ethylcellulose and α-terpinol. For a good homogenization, both solutions were placed in the ball mill (*Lab Mills lx QM vertical planetary ball mill*) at a frequency of 40 kHz for 14 h.

(ii) The next step was to deposit the TiO_2 and $CuMnO_2$ films on the FTO support. Therefore, the FTO was cleaned with acetone, ethanol and DI water in an ultrasonic bath, followed by treatment for 20 min in UV ozone cleaner (*Ossila Producer*). The deposition of the thin and transparent TiO_2 film on the FTO support was achieved with the conventional doctor blade method, using the previously obtained TiO_2 solution. The as-obtained structure, FTO-TiO_2, was dried for 30 min to 60 °C, and calcinated at 450 °C for 1 h. The last step, the deposition of the thin and transparent $CuMnO_2$ film on the FTO-TiO_2 structure, was achieved, to fabricate the UV photodetector. Deposition of $CuMnO_2$ thin films using the spin coating method (*WS-400-6NPPB Spin Coater, Laurell Technology Corporation*) presumes the mixing of a homogenized $CuMnO_2$ solution with ethyl alcohol and deposition twice for 30 s with a speed rotation of 4000 rpm. For the removal of the organic compounds used in the homogenization solution matrix, and to facilitate the adhesion of the $CuMnO_2$ film to the TiO_2 film, a thermal treatment of 250 °C was applied for 1 h. The collection of electrical data was performed by means of metal wires affixed with silver paste. One wire was placed on the FTO and the other on the $CuMnO_2$ film.

2.3. Materials and Electrical Characterization

The crystalline structure of the films was characterized by X-ray diffraction (*XRD, PANalytical X'Pert PRO MPD Diffractometer, Almelo, The Netherlands*) with Cu-Kα radiation in the range *2theta* = 20–80°. The morphology of the layers and films was examined using scanning electron microscopy (*SEM, FEI Inspect S model, Eindhoven, The Netherlands*), coupled with the energy dispersive X-ray analysis detector (EDX) for elemental analysis of the as-synthesized samples. Atomic force microscopy (*AFM, Model Nanosurf® EasyScan 2 Advanced Research, Liestal, Switzerland*), with non-contact mode (scan size of 1 μm × 1 μm,) was used to determine particle sizes on the surface, surface roughness and topographical parameters *Sp* and *Sv*, necessary for the calculation of thickness films. The optical properties of the as-synthesized samples were recorded using UV-VIS analysis (*PerkinElmer Lambda 950 UV/Vis spectrophotometer, Shelton, CT, USA*) with an integrating sphere, in the range of 300–600 nm. The band gap *Eg* of the semiconductor materials was determined by plotting the Kubelka–Munk function against energy (eV).

Electrical measurements of the obtained photodetectors were performed using the Keithley 2450 SourceMeter SMU Instruments (*Keithley Company, Cleveland, OH, USA*). I-V measurements were performed to test the functionality in dark and UV illumination of the "*n-p*" heterojunction between *n*-TiO_2 and *p*-$CuMnO_2$. The measurements were made in direct polarization at a voltage between −1 V and 1 V with a step rate of 10 mV/s. Ultraviolet detection characteristics were evaluated by recording the current as a function of time, both in 0 V self-power mode and in 1 V power mode in the dark and under lamp illumination at 365 nm with a light power of 0.1 mW/cm^2. The calibration of the UV lamp power was performed using a Solar 4000 sensor device (AMPROBE) (*Octopart Inc., New York, NY, USA*).

3. Results and Discussion

3.1. Structural and Morphological Properties

Figure 2 shows the XRD spectra for the FTO-TiO_2 film and the as-synthesized FTO-TiO_2-$CuMnO_2$ films. The results presented show that microwave-assisted hydrothermal treatment for TiO_2 synthesis was determined to obtain a rutile crystalline form, confirmed by the main peaks at *2theta*: 27.65°, 32.47°, 54.64° (JCPDS 01-073-1764). For the $CuMnO_2$ powder, the XRD pattern confirms the crednerite phase identified by the main peaks at *2theta*: 31.32°, 33.45°, 37.0°, 52.42°, 56.85° (JCPDS 01-075-1010) [23]. Additionally, the main peaks for FTO were identified at *2theta*: 26.67°, 33.90°, 37.96°, 51.84°, 61.87°,65.85° (JCPDS 01-077-0448). Based on X-ray analysis, the average crystallite sizes were calculated by the Debye–Scherrer formula and were estimated to be about 20.80 nm for TiO_2 and 11.10 nm for $CuMnO_2$, respectively. In the XRD pattern of the FTO-TiO_2-$CuMnO_2$ heterostructure, the peaks referring to the phases of $CuMnO_2$ and TiO_2 are preserved, and the successful synthesis of the crystalline *n*-TiO_2/*p*-$CuMnO_2$ heterojunction is confirmed.

The SEM images of the TiO_2 (Figure 3a) and $CuMnO_2$ (Figure 3b) powders exhibited a spherical morphology for TiO_2 nanoparticles, and homogenous and uniformly crystals for $CuMnO_2$ pristine, respectively. Figure 3c–e presents the surface morphologies for TiO_2 film (Figure 3c), $CuMnO_2$ film (Figure 3d) and the interface between the TiO_2 and $CuMnO_2$ films (Figure 3e). From the analysis of the SEM images, it can be evidenced that the TiO_2 film is deposited uniformly on FTO, without agglomeration and cracks (Figure 3c). Moreover, the $CuMnO_2$ film is deposited uniformly on FTO-TiO_2 and presents the same morphological characteristics as the TiO_2 film (Figure 3d). EDX analysis (Figure 3f,g) confirms the presence of chemical elements: Si, Sn, Ti and O from the FTO-TiO_2 structure (Figure 3f), and Si, Sn, Ti, O, Cu and Mn from the FTO-TiO_2-$CuMnO_2$ structure, respectively (Figure 3g).

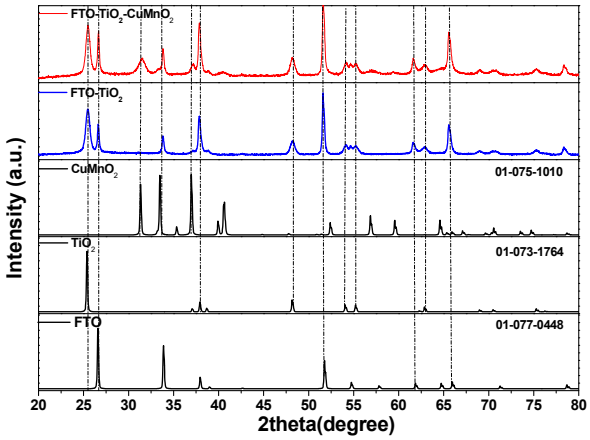

Figure 2. X-ray patterns for the FTO-TiO_2-$CuMnO_2$ heterostructures.

The surface morphologies by AFM analysis for the structures FTO-TiO_2 and FTO-TiO_2-$CuMnO_2$ are shown in Figure 4a,b. AFM surface morphologies confirm the results obtained by the related SEM images, for both structures. For the determination of the particle sizes on the surface films, Nanosurf EasyScan2 software was used. The particle sizes determined by AFM and XRD techniques are in accordance with each other, and the size ratio is preserved, but with some differences due to the different calculation algorithms used for each technique. The surface roughness was measured on a surface area of approximately 1.326 pm^2 and was determined from the values of *Sa* (average roughness) and *Sq* (the mean square root roughness). Topographical parameters *Sp* (the maximum peak height deviation of the roughness) and *Sv* (the maximum valley depth deviation of the roughness) were used for the calculation of the layers' thicknesses [22,24,25]. All the obtained data are presented in Table 1.

Table 1. Surface particle size, nano-roughness and layer thickness.

Sample	Particle Size (nm)	*Sa* (nm)	*Sq* (nm)	*Sp* (nm)	*Sv* (nm)	Layer Thickness *Sp*-*Sv* (nm)
FTO-TiO_2	65	18.99	23.948	85.265	−77.617	162.882
FTO-TiO_2-$CuMnO_2$	47	24.452	31.068	82.229	−109.28	191.509

3.2. Optical and Electrical Characteristics

To confirm the transparency characteristic of the heterostructure devices, UV-VIS spectroscopy analysis was used for FTO-TiO_2 and FTO-TiO_2-$CuMnO_2$, as shown in Figure 5a,b respectively. The UV-VIS spectra indicate the transparency of the devices in the visible light region, which is attributed to the wide band gap of TiO_2 (3.38 eV) and $CuMnO_2$ (3.31 eV). The light transmittance pattern decreases when a thin film of $CuMnO_2$ is deposited on top, with an average visible light transparency of 60%, 10% lower than for the FTO-TiO_2, this being generated by the increase in the total thickness of the layers (Figure 5a). According to Nguyen et al., a 40% transparency requirement for applications in window-type sensors must be accomplished by films [12]. In this way, both as-synthesized films demonstrate an average transmittance higher than the 40% transparency requirement.

In Figure 5b, a maximum absorption region at near 330 nm can be seen and presents a decrease at around 385 nm wavelengths for both samples. This is due to the strong absorption spectra of TiO_2 film and *n*-TiO_2/*p*-$CuMnO_2$ heterojunction attributed to the electron transition from the valence band to the conduction band. This points to the high absorption selectivity of UV radiation for sensors and power generation.

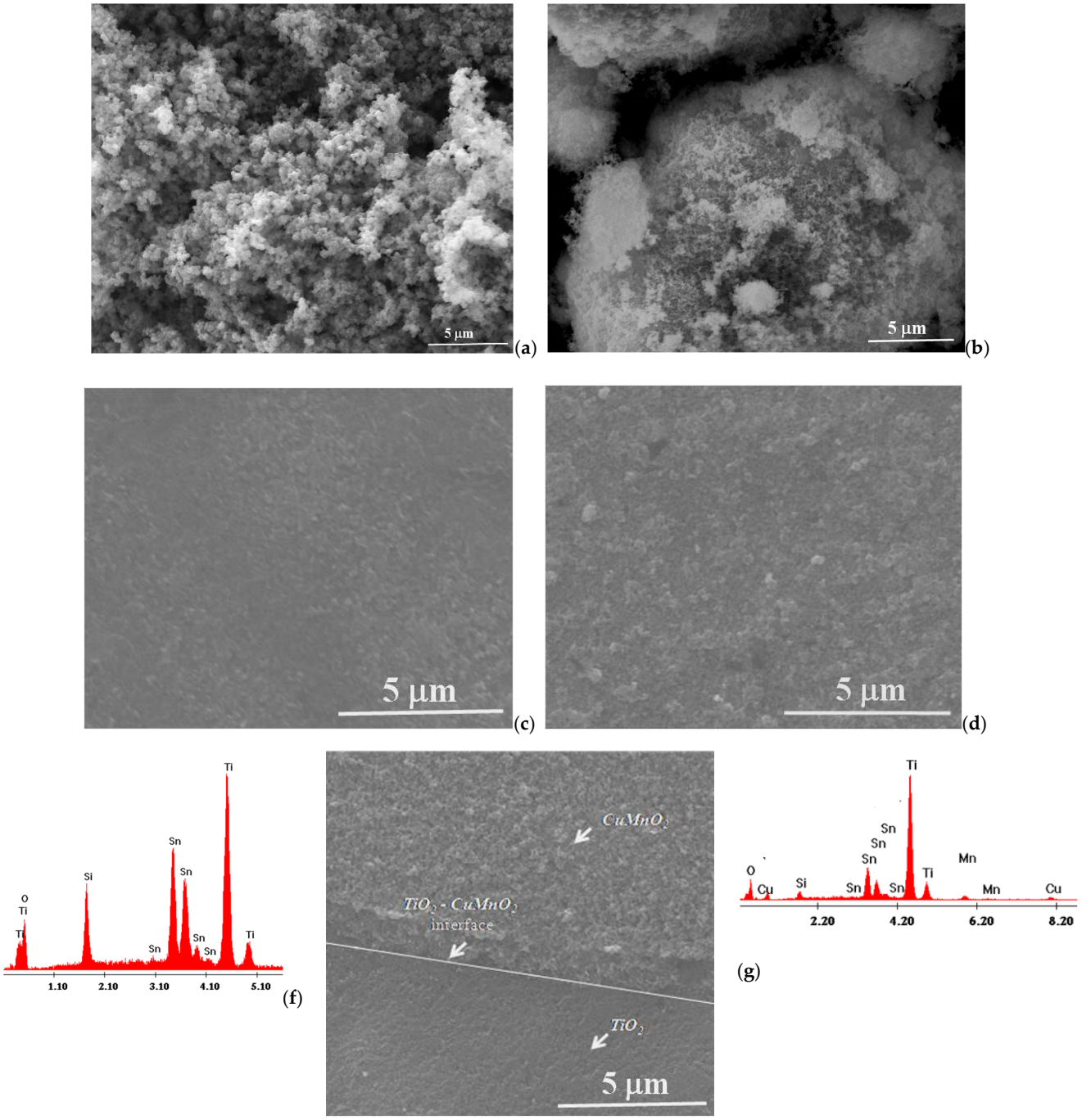

Figure 3. SEM images of the TiO_2 (**a**) and $CuMnO_2$ powders (**b**); TiO_2 (**c**) and $CuMnO_2$ films (**d**); interface TiO_2-$CuMnO_2$ films (**e**); EDX spectra of the FTO-TiO_2 (**f**) and FTO-TiO_2-$CuMnO_2$ (**g**) structures.

The current–voltage measurement in the dark and under UV illumination is presented in Figure 6a, when an increase in current in the forward bias by the UV illumination from 196 nA (DARK state) to 283 nA (UV state) was generated. Moreover, under UV illumination, a reduction in the turn-on voltage is shown, almost half from the dark state of 0.43 V to 0.24 V. This aspect confirms that the heterojunction under UV illumination decreases the power consumption of the junction.

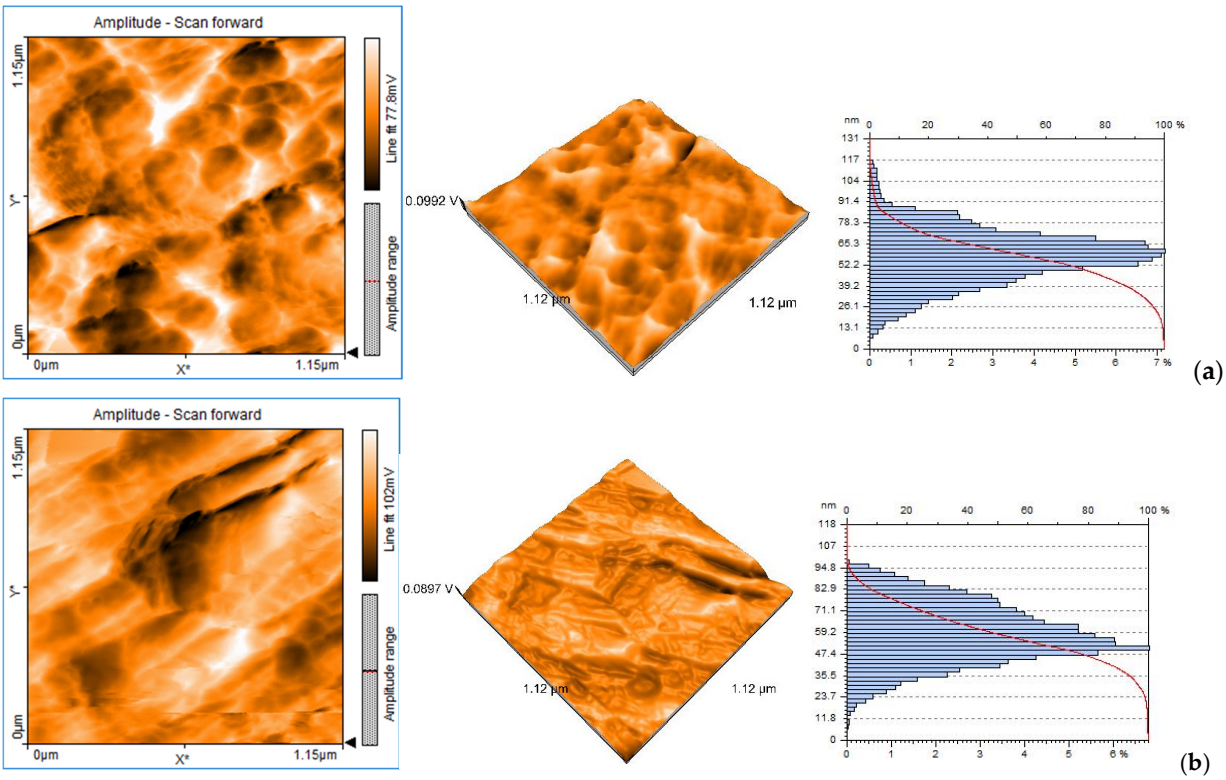

Figure 4. Two-dimensional and 3D AFM surface images and particle size distribution for FTO-TiO_2 film (**a**) and FTO-TiO_2-$CuMnO_2$ film (**b**).

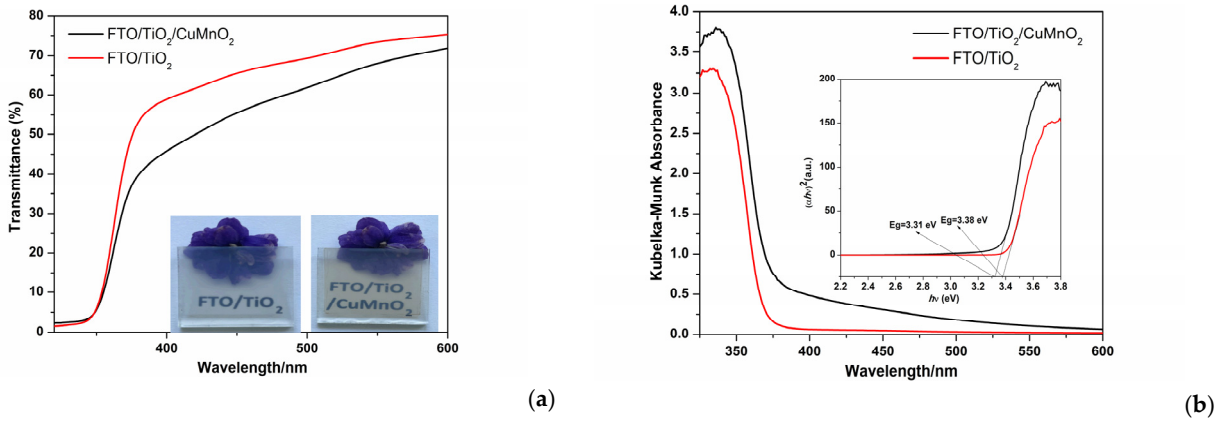

Figure 5. Transmittance spectra and pictures of FTO-TiO_2 and FTO-TiO_2-$CuMnO_2$ transparent films (**a**); *Kubelka–Munk* absorption and Tauc's plot for *Eg* calculation (**b**).

The *I-V* characteristics of TiO_2 and $CuMnO_2$ thin films deposited on the FTO substrate with silver contact confirm the rectifying nature of the *n-p* junction, and an increase in the asymmetry between the forward and reverse biases in photo illumination suggests a higher rectification behavior under UV exposure.

To evaluate the *I-V* characteristics of the *n-p* junction, the thermionic emission current–voltage relation was used, expressed by Equation (1).

$$I = I_0 \left[\exp\left(V/n\,k\,T\right) - 1\right] \quad (1)$$

where T is the temperature in Kelvin (298 K), k is the Boltzmann constant (1.6×10^{-19} C), n is the ideality factor, V is the applied voltage, and I_0 is the reverse saturation current.

The reverse saturation current (I_0) and the ideality factor (n) can be calculated from the intercept and slope of the straight-line region of the forward bias in the *Log (I)–V* plot, presented in Figure 6b. Based on the literature data, a previous report on the $TiO_2/CuMnO_2$ heterojunction has shown that the ideality factor is between 3.95 and 6.48 depending on the process parameters of the experimental program [21,22]. The heterojunction parameters of FTO-TiO_2-$CuMnO_2$ under both dark and UV illumination conditions are presented in Table 2, where I_F and I_R are the current under forward and reverse bias, respectively, and V_T is the turn-on voltage. The ideality factor n = 5.58 is greater than its normal range ($1 < n < 2$) [26]. Considering that thermionic emission is responsible for carrier recombination at the junction but does not drive the transport mechanism, it can be argued that this is determined by defects of the quasi-neutral zone and the junction [27].

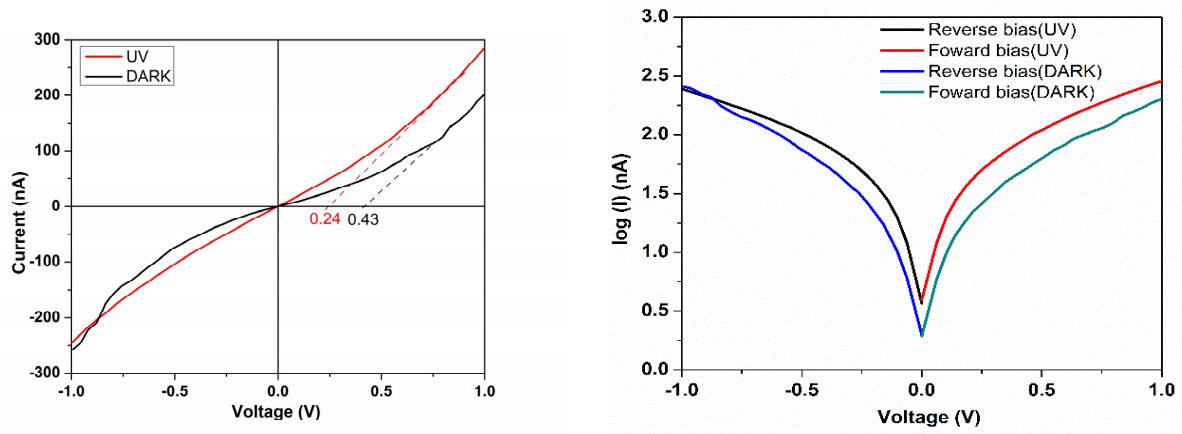

(**a**) (**b**)

Figure 6. Current–voltage characteristics of the transparent heterojunction of n-TiO_2/p-$CuMnO_2$ under dark and UV illumination (**a**); *Log* of forward and reverse bias under dark and UV-illuminated conditions. (**b**).

Table 2. Electrical parameters of the FTO-TiO_2-$CuMnO_2$ photodetector.

Sample	Type	V_T (V)	I_F (A)	I_R (A)	n	I_0 (A)
1 V bias FTO-TiO_2-$CuMnO_2$	Dark	0.43	196×10^{-9}	257×10^{-9}	5.58	1.35×10^{-9}
	UV	0.24	283×10^{-9}	245×10^{-9}	-	1.90×10^{-9}

The photocurrent measurement in the dark for the self-powered mode was approximately −0.3 nA, and when the photodetector was illuminated for 20 s with a UV light intensity of 0.1 mW/cm^2, a self-powered current of 14.2 nA was generated; the results are presented in Figure 7.

The sensitivity of the photodetector at the 0 bias was calculated from the ON/OFF ratio (I_{UV}/I_{DARK}) of approximately 48.3, much higher than for the 1 V bias when it was detected as approximately 1.4 [28]. Responsivity values were calculated using Equation (2) [29]

$$R = (I_{UV} - I_{DARK})/P_{opt}\, S \quad (2)$$

where I_{UV} is the photocurrent under UV lighting, I_{DARK} is the current in the dark, S is the effective area (2 cm^2) and P_{opt} is the optical power of the UV source (0.1 mW/cm^2). From Equation (2), the responsivity value of the thin film $TiO_2/CuMnO_2$ heterojunction photodetector in self-powered mode is 2.84×10^7 A W^{-1} cm^2, and in 1 V bias mode it is 1.82×10^6 A W^{-1} cm^2.

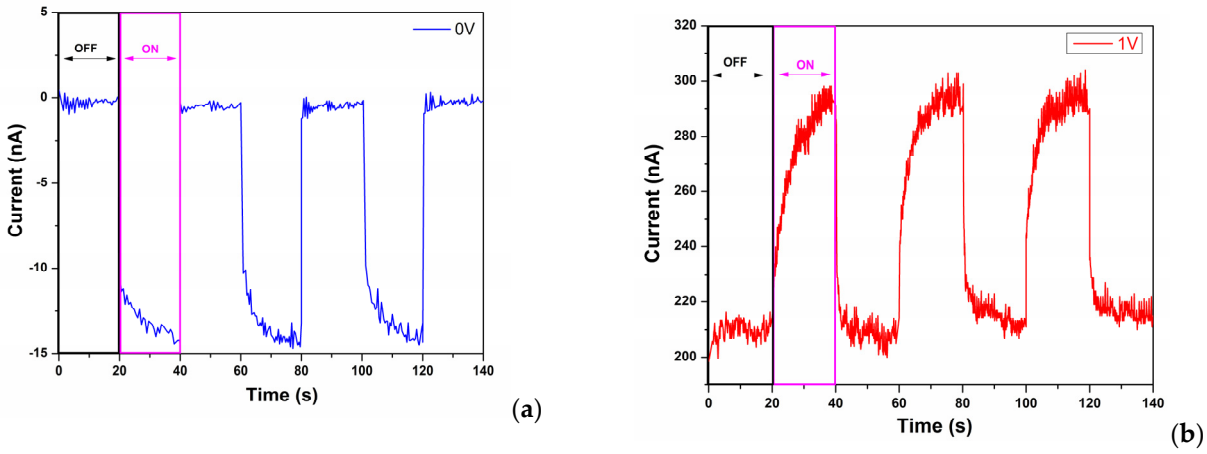

Figure 7. UV time-dependent photoresponse properties of the sensors. (**a**) Response of the sensor in self-powered mode; (**b**) UV response of the sensor at 1 V bias voltage.

The response time was calculated from the time taken to increase from 10% to 90% of the photocurrent, and the recovery time from the time taken to decrease from 90% to 10% of its maximum value [4]. For the self-powered mode, the response time is 7.3 s and the recovery time is 0.4 s, and in 1 V bias mode the response time is 15.16 s and the recovery time is 2.18 s.

Although junctions built in two-dimensional layers have a theoretical surface area smaller than junctions built in one-dimensional or mixed layers, because the size of both the TiO_2 and $CuMnO_2$ crystallites is very small, both of the contact surfaces at the interfaces between oxides and with O_2 (gas) and O_2^- (ads) increase the effective active area at a level almost similar to other techniques. This higher surface area increases electron hole pairs generation without applying an external current (0 V bias) to the FTO-TiO_2-$CuMnO_2$ photodetector [1]. The higher oxygen absorption–desorption process is facilitated by the crednerite layer due to the small nanosize of the crystals and the relatively rough surface obtained after deposition [23]. Figure 8 presents a schematic representation of the detection process under dark (Figure 8a) and ultraviolet (UV) (Figure 8b) irradiation conditions for a bilayer heterostructure device. Furthermore, in Figure 8a,b, the band diagram of the current conduction mechanism at the surface interface of the $CuMnO_2$ and TiO_2-$CuMnO_2$ junction interface under dark and illumination conditions at 0 V bias is presented.

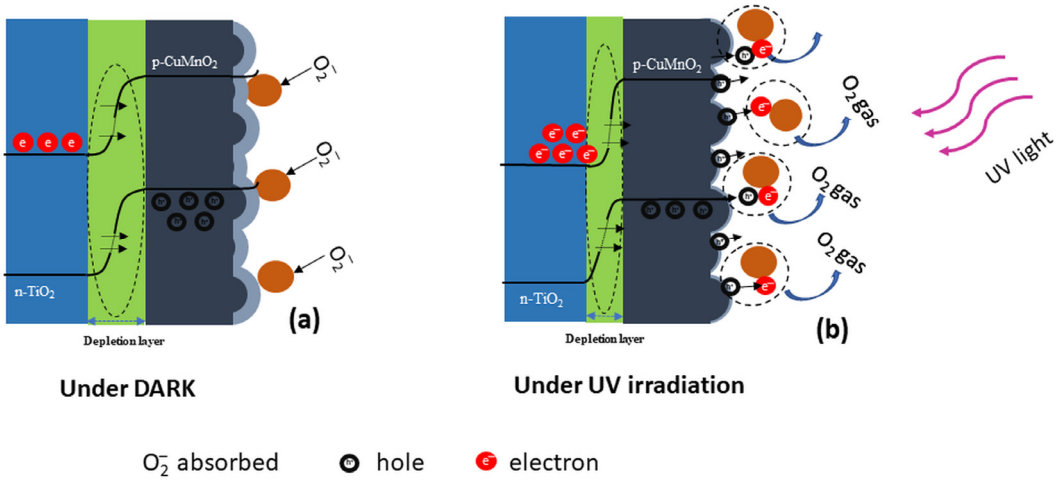

Figure 8. FTO-TiO_2-$CuMnO_2$ in darkness (**a**); FTO-TiO_2-$CuMnO_2$ in UV irradiation (**b**); band diagram of the FTO-TiO_2-$CuMnO_2$ device at 0 V (**a**) in darkness and (**b**) under UV irradiation.

In the dark state, oxygen atoms from the atmosphere interact with the free holes presented in *p*-type $CuMnO_2$ and the adsorbed oxygen ions, and due to the high surface area, oxygen molecules are adsorbed on the surface of the crednerite layer, which introduces a potential barrier (Figure 8a). Thus, a high-conductivity hole accumulation region is formed on the surface of the $CuMnO_2$ layer, according to the following Equation (3) [18]

$$O_2\ (gas) \boxplus O^-\ (ads) + h^+ \quad (3)$$

This generates a downward band of the energy band on the surface of *p*-$CuMnO_2$, as shown in Figure 8a. The light absorption process occurs under UV illumination (Figure 8b) when the photon energy generated is greater than the band gap value. Some of the photons generated by UV illumination are absorbed by photosensitive semiconductors and the generated energy excites the electron in the valence band and is launched to the conduction band; this generates many electrons hole pairs in the heterojunction interface of the TiO_2 layer, and the photogenerated holes go to the $CuMnO_2$ surface [12]. These holes are trapped by adsorbed oxygen molecules on the surface of $CuMnO_2$ and, therefore, the desorption process happens, releasing oxygen and narrowing the depletion zone and lowering the heterojunction interface. The photogenerated recovery of O_2^- to O_2 (g) is represented by the following Equation (4) [18]

$$O_2^-(abs\cdot) + h^+ \rightarrow O_2\ (gas) \quad (4)$$

Therefore, due to the high specific surface area of $CuMnO_2$, an increased number of oxygen molecules are adsorbed and, therefore, a larger number of photogenerated holes are trapped by the adsorbed oxygen on the surface of $CuMnO_2$. The electron hole recombination process is narrowed, and a greater separation of the charge carriers is generated, resulting in a good photoconductivity of the photodetector device [12]. The self-powered photovoltaic device based on *n*-TiO_2/*p*-$CuMnO_2$ heterojunction is transparent, also due to the broad energy band gap of the metal oxide semiconductor used as presented in Figure 5.

4. Conclusions

A self-powered photodetector with the configuration FTO/*n*-TiO_2/*p*-$CuMnO_2$ was successfully achieved for the first time, to the best of our knowledge, by using a layer-by-layer technique and doctor blade and spin coating methods. The structural and morphological characteristics of the FTO/*n*-TiO_2/*p*-$CuMnO_2$ structures confirmed the phases' stability and purity as well as being uniformly covered, without cracks of the synthesized thin and transparency films. Due to the alignment of the band and the transparency of the layers, a device based on the *n-p* junction was demonstrated to operate without an external voltage bias. The device shows an excellent ON/OFF ratio at 0 bias of about 48.3, much higher than that for the 1 V bias of about 1.4. Moreover, good responsivity values under low ultraviolet illumination in both modes was calculated. The response and recovery times are relatively slower for both modes due to the slow mobility of the photogenerated holes in the *n-p* depletion layer; instead, when the 0 V bias is applied, these times improve and are faster. The above results show that the transparent heterojunction device of *n*-TiO_2/*p*-$CuMnO_2$ exhibited a self-powered ultraviolet photodetector with high sensitivity.

Author Contributions: C.L. was involved in conceptualization, methodology, investigation, writing—original draft; M.N. was involved in conceptualization, methodology, investigation, writing—original draft; C.O. was involved in conceptualization, methodology, investigation, writing—original draft; V.Ş. was involved in validation, investigation, writing—original draft; C.B. was involved in methodology, investigation, writing—original draft, supervision. All authors have read and agreed to the published version of the manuscript.

Funding: This research was funded by a grant of the Ministry of Research, Innovation and Digitization, CNCS–UEFISCDI, project number PN-III-P1-1.1-TE-2021-0963, within PNCDI III, with contract number TE13/2022 (DD-CyT) and project code PN 19 22 04 01 TINSME, 40 N/2019, and partially by project number PN-III-P2-2.1-PED-2019-4492, contract number 441PED/2020 (3DSAPECYT).

Institutional Review Board Statement: Not applicable.

Informed Consent Statement: Not applicable.

Data Availability Statement: Not applicable.

Acknowledgments: Authors would like to acknowledge the support provided by Maria Poienar in delivering the $CuMnO_2$ powder used in the experiments and Mihaela Birdeanu for AFM measurements.

Conflicts of Interest: The authors declare no conflict of interest.

References

1. Chetri, P.; Dhar, J.C. Self-powered UV detection using SnO_2 nanowire arrays with Au Schottky contact. *Mater. Sci. Semicond. Process.* **2019**, *100*, 123–129. [CrossRef]
2. Chen, H.; Liu, K.; Hu, L.; Al-Ghamdi, A.A.; Fang, X. New concept ultraviolet photodetectors. *Mater. Today* **2015**, *18*, 493–502. [CrossRef]
3. Patel, M.; Kim, H.S.; Kim, J. All transparent metal oxide ultraviolet photodetector. *Adv. Electron. Mater.* **2015**, *1*, 1500232. [CrossRef]
4. Cui, S.; Liang, D.; Liu, M.; Vivo, P.; Zheng, M.; Zhuang, T.; Sun, Q.; Yang, W.; Zhang, H. From transistors to phototransistors by tailoring the polymer stacking. *Adv. Electron. Mater.* **2022**, 2200019. [CrossRef]
5. Zou, Y.; Zhang, Y.; Hu, Y.; Haoshuang, G. Ultraviolet Detectors Based on Wide Bandgap Semiconductor Nanowire: A Review. *Sensors* **2018**, *18*, 2072. [CrossRef]
6. Abbas, S.; Kim, J. All-metal oxide transparent photodetector for broad responses. *Sens. Actuators A: Phys.* **2020**, *303*, 111835. [CrossRef]
7. Praveen, S.; Veeralingam, S.; Badhulika, S. A Flexible Self-Powered UV Photodetector and Optical UV Filter Based on β-Bi_2O_3/SnO_2 Quantum Dots Schottky Heterojunction. *Adv. Mater. Interfaces* **2021**, *8*, 2100373. [CrossRef]
8. Yang, X.; Guo, J.; Zhang, Y.; Liu, W.; Sun, Y. Hole-selective NiO:Cu contact for NiO/Si heterojunction solar cells. *J. Alloys Compd.* **2018**, *747*, 563–570. [CrossRef]
9. Krysova, H.; Zlamalova, M.; Tarabkova, H.; Jirkovsky, J.; Frank, O.; Kohout, M.; Kavan, L. Rutile TiO_2 thin film electrodes with excellent blocking function and optical transparency. *Electrochim. Acta* **2019**, *321*, 134685. [CrossRef]
10. Zhang, D.; Gu, X.; Jing, F.; Gao, F.; Zhou, J.; Ruan, S. High performance ultraviolet detector based on TiO_2/ZnO heterojunction. *J. Alloys Compd.* **2015**, *618*, 551–554. [CrossRef]
11. Yin, B.; Zhang, Y.; Li, K.; Zhou, J.; Liu, C.; Zhang, M.; Ruan, S. UV detector based on an FTO/TiO_2/MoO_3 heterojunction with a potential well trapping electrons in the dark. *Nanotechnology* **2019**, *30*, 465501. [CrossRef] [PubMed]
12. Nguyen, T.T.; Patel, M.; Kim, S.; Mir, R.A.; Yi, J.; Dao, V.-A.; Kim, J. Transparent photovoltaic cells and self-powered photodetectors by TiO_2/ NiO heterojunction. *J. Power Sources* **2021**, *481*, 228865. [CrossRef]
13. Bai, Z.M.; Yan, X.Q.; Chen, X.; Liu, H.S.; Shen, Y.W.; Zhang, Y. ZnO nanowire array ultraviolet photodetectors with self-powered properties. *Curr. Appl. Phys.* **2013**, *13*, 165–169. [CrossRef]
14. Xie, Y.; Wei, L.; Wei, G.; Li, Q.; Wang, D.; Chen, Y.; Yan, S.; Liu, G.; Mei, L.; Jiao, J. A self-powered UV photodetector based on TiO_2 nanorod arrays. *Nanoscale Res. Lett.* **2013**, *8*, 188. [CrossRef] [PubMed]
15. Xiong, D.H.; Zhang, W.J.; Zeng, X.W.; Xu, Z.; Chen, W.; Cui, J.; Wang, M.K.; Sun, L.C.; Cheng, Y.B. Enhanced performance of p-type dye-sensitized solar cells based on ultrasmall Mg-doped $CuCrO_2$ nanocrystals. *Chem. Sus. Chem.* **2013**, *6*, 1432–1437. [CrossRef]
16. Wang, L.; Arif, M.; Duan, G.R.; Chen, S.M.; Liu, X.H. A high performance quasi-solid- state supercapacitor based on $CuMnO_2$ nanoparticles. *J. Power Sources* **2017**, *355*, 53–61. [CrossRef]
17. Amrute, A.P.; Lodziana, Z.; Mondelli, C.; Krumeich, F.; Perez-Ramirez, J. Solid-state chemistry of cuprous delafossites: Synthesis and stability aspects. *Chem. Mater.* **2013**, *25*, 4423–4435. [CrossRef]
18. Hsu, C.-L.; Chang, E.-C.; Hsueh, H.-T.; Liu, Y.-H. Solution-synthesized *p*-type $CuMnO_2$ and *n*-type ZnO to form the core-shell nanowires for photo and gas sensing. *J. Alloys Compd.* **2022**, *899*, 163380. [CrossRef]

19. Zhang, Y.; Xu, J.; Shi, S.; Gao, Y.; Wang, C.; Zhang, X.; Yin, S.; Li, L. Development of solution-processed ZnO nanorod arrays-based photodetectors and the improvement of UV photoresponse via AZO seed layers. *ACS Appl. Mater. Interfaces* **2016**, *8*, 22647–22657. [CrossRef]
20. Prabhu, R.R.; Saritha, A.C.; Shijeesh, M.R.; Jayaraj, M.K. Fabrication of p-CuO/n-ZnO heterojunction diode via sol-gel spin coating technique. *Mater. Sci. Eng. B* **2017**, *220*, 82–90. [CrossRef]
21. Lazau, C.; Poienar, M.; Orha, C.; Ursu, D.; Nicolaescu, M.; Vajda, M.; Bandas, C. Development of a new "n-p" heterojunction based on TiO_2 and $CuMnO_2$ synergy materials. *Mat. Chem. Phys.* **2021**, *272*, 124999. [CrossRef]
22. Nicolaescu, M.; Bandas, C.; Orha, C.; Şerban, V.; Lazău, C.; Căprărescu, S. Fabrication of a UV photodetector based on *n*-TiO_2/*p*-$CuMnO_2$ heterostructures. *Coatings* **2021**, *11*, 1380. [CrossRef]
23. Poienar, M.; Banica, R.; Sfirloaga, P.; Ianasi, C.; Mihali, C.V.; Vlazan, P. Microwave-assisted hydrothermal synthesis and catalytic activity study of crednerite-type $CuMnO_2$ materials. *Ceram. Int.* **2018**, *44*, 6157–6161. [CrossRef]
24. Skoneczny, W.; Niedzwiedz, M.; Bara, M. The Effect of production parameters of oxide layers on their nanostructure, nanomorphology, and surface free energy. *Appl. Sci.* **2018**, *8*, 2251. [CrossRef]
25. Birdeanu, A.-V.; Birdeanu, M.; Fagadar-Cosma, E. Corrosion protection characteristics of ceramics, porphyrins and hybrid ceramics/porphyrins, deposited as single and sandwich layers, by pulsed laser deposition (PLD). *J. Alloy Compd.* **2017**, *706*, 220–226. [CrossRef]
26. Shi, Z.F.; Xu, T.T.; Wu, D.; Zhang, Y.T.; Zhang, B.L.; Tian, Y.T.; Li, X.J.; Du, G.T. Semi-transparent all-oxide ultraviolet light-emitting diodes based on ZnO/NiO-core/shell nanowires. *Nanoscale* **2016**, *8*, 9997–10003. [CrossRef]
27. Hasan, M.R.; Xie, T.; Barron, S.C.; Liu, G.; Nguyen, N.V.; Motayed, A.; Rao, M.V.; Debnath, R. Self-powered p-NiO/n-ZnO heterojunction ultraviolet photodetectors fabricated on plastic substrates. *APL Mater* **2015**, *3*, 106101. [CrossRef]
28. Gao, Y.; Xu, J.; Shi, S.; Dong, H.; Cheng, Y.; Wei, C.; Zhang, X.; Yin, S.; Li, L. TiO_2 nanorod arrays based self-powered UV photodetector: Heterojunction with NiO nanoflakes and enhanced UV photoresponse. *ACS Appl. Mater. Interfaces* **2018**, *10*, 11269–11279. [CrossRef]
29. Ranjith, K.S.; Kumar, R.T. Facile construction of vertically aligned ZnO nanorod/PEDOT:PSS hybrid heterojunction-based ultraviolet light sensors: Efficient performance and mechanism. *Nanotechnology* **2016**, *27*, 95304. [CrossRef]